CHAPTER 3

DESIGN AND DEVELOPMENT OF TM_{01} TO TE_{11} SWG MODE CONVERTER

3.1 Design Methodology of SWG Mode Converter

3.2 Experimental Setup

3.3 Results and Discussion

3.4 Conclusions

*Part of this work has been accepted as:

Kumar V., Dwivedi S. and Jain P.K., "Experimental Investigation and Design of Sectoral Waveguide TM_{01} to TE_{11} Mode Converter," accepted for publication in *Journal of Microwave Power and Electromagnetic Energy*, 2019.

As we have discussed in previous Chapters that the SWG mode converter which is an HPM component mostly used in HPM systems between HPM source and antenna and often used for conversion from *TEM* mode to TE_{11} mode. Using mode converters, HPM system enables to radiate its maximum RF power on the axis of propagation, otherwise, there is null in radiation pattern at this axis. At the high-temperature incorporation of dielectric material to supports, the mode conversion decreases the high power capability of the SWG mode converter and unable to sustain at very high temperature as reported by Chittora *et al.* (2016). Because dielectric deform its structure at high temperature and unable to recover its previous structure precisely, and this characteristic affects the mode converter performance. The SWG mode converter is an all-metal structure which can handle heat transfer and capability to sustain at higher temperatures. These mode converters are used with the HPM sources, e.g. magnetic-insulated transmission-line oscillator (MILO), relativistic-backward oscillator (RBWO), relativistic-klystron oscillator (RKO) and virtual cathode oscillator (VIRCATOR); radiate RF energy in azimuthally symmetrical modes such as *TEM* or TM_{01}.

The research reported by Somov *et al.* (1998) and Yuan *et al.* (2005) focused on all metal SWG mode converter designs are to reduce the insertion loss due to axial discontinuity. The technique reported in these two manuscripts is limited to mode conversion from *TEM* to TE_{11} mode conversion. In this chapter, the SWG mode converter structure is proposed with modification for beam stability and TM_{01} to TE_{11} mode conversion. A practical S-band sectoral waveguide mode converter has been designed, optimised and experimented for its performance. The optimised mode converter design's parameters are predicted analytically and are used in fabrication and simulation. The performance of the simulated design of the SWG mode converter is compared with fabricated design and found good in the agreement.

3.1. Design Methodology of SWG Mode Converter

For the design of TM_{01} to TE_{11} SWG mode converter, an additional waveguide section which transforms TM_{01} into TE_{11} mode is required to be added in the SWG mode converter of Figure 3.1. A coaxial guide with the tapered central conductor, for impedance matching, transforms TM_{01} into the TE_{11} mode. Such a section has been added both sides, transform TM_{01} to TE_{11} mode with proper impedance matching as shown in Figure 3.1.

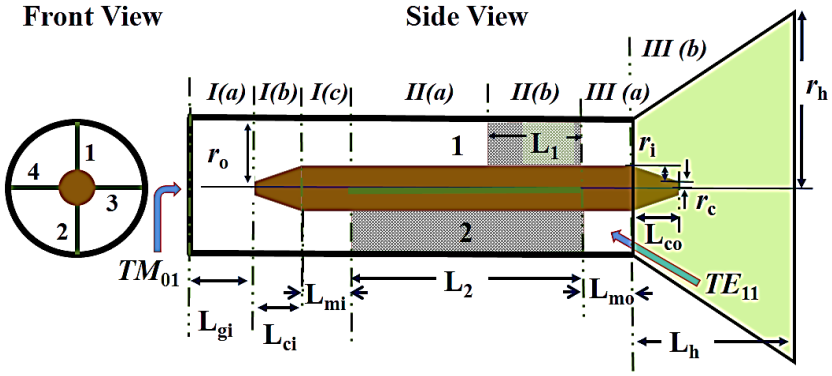

Figure 3.1. Proposed modified SWG mode converter for TM_{01} to TE_{11} mode conversion.

At the input port TM_{01} mode feed in the circular waveguide of Region *I (a)*. The tapered section of an inner conductor of Region *I (b)* is converting TM_{01} mode to *TEM* mode, and similar conversion also reported using step discontinuity (Tribak *et al*. 2013). From Region *I (c)* to *III (a)* working is similar to SWG Mode Converter (*TEM* to TE_{11}) discussed in section 1.4, only the Region *II (b)* is added new. Region *III (b)* provides impedance matching between the coaxial waveguide to coaxial horn antenna.

Designing SWG mode converter (TM_{01} to TE_{11}) involves various design constraints such as cutoff frequencies of each region, overall mode conversion efficiency, the structure bandwidth, and beam stability at the output port. In the SWG mode converter the radius of the inner conductor (r_i) and length of mode conversion region $L(=L_2-L_1)$ belongs to Region *II(a)*, as shown in Figure 1, are the prime

parameters. The inner conductor radius (r_i) chosen such as it can fulfil the condition, that cut-off frequency of $SWG_{\pi/2}$ for TE_{11} mode should below than the source frequency and cut-off frequency of SWG_{π} of TE_{31} mode be higher than the source frequency $(f_c|_{TE11}^{SWG\pi/2} < f_0 < f_c|_{TE31}^{SWG\pi})$. This ensures that all the SWGs in the design are allowing only TE_{11} mode. Since the sectoral angle of upper half (SWG_{π}) and lower half ($SWG_{\pi/2}$) waveguides are different, therefore propagation constants $(\beta_1 \text{ and } \beta_2)$ yield phase difference in between them. In order to get π rad phase difference, length of the Region *II(a)* $L_2 - L_1$, used in an expression (1.6) becomes:

$$(L_2 - L_1) = \pi / (\beta_1 - \beta_2) \quad . \tag{3.1}$$

Eigenmode, cutoff frequencies and guide wavelength of the different region of the SWG converter can be obtain using SWG dispersion expression reported by Zhang *et al.* (2008). Now, the length of each region is calculated as per the design algorithm is given in Figure 2. In order to reduce mismatch reflections due to insertion of the SWG mode converter with the circuit, the outer conductor radius (r_0) of mode converter is also taken the same as the source structure radius. The tapered section (r_c) radius is taken as $r_i / 6$ at both inner conductor end.

Length of Region *I(a)* L_{gi} is taken a quarter guide wavelength whereas the length of Region *I(b)* (L_{ci}) is optimized close to TM_{01} mode half wavelength. The optimum length of *Plate1* is obtained in the range $0.4\lambda_g^{TE11} < L_1 < 0.6\lambda_g^{TE11}$ (close to the half-wavelength). Further, length of Region *III(b)* (L_{co}) is taken as half-wavelength whereas the length and radius of horn antenna are chosen as per directivity requirement. Matlab code is written for calculating the radial propagation constant, axial propagation constant and length $L_2 - L_1$. The input parameters are shown in Table 3.1.

Table 3.1. Input parameters for the SWG mode converter design

Parameter	Values	Parameter	Values
f_o	3 GHz	r_c	5.0 mm
r_o	57.5 mm	β_1	0.0585074 rad/mm
r_i	30.0 mm	β_2	0.0410930 rad/mm

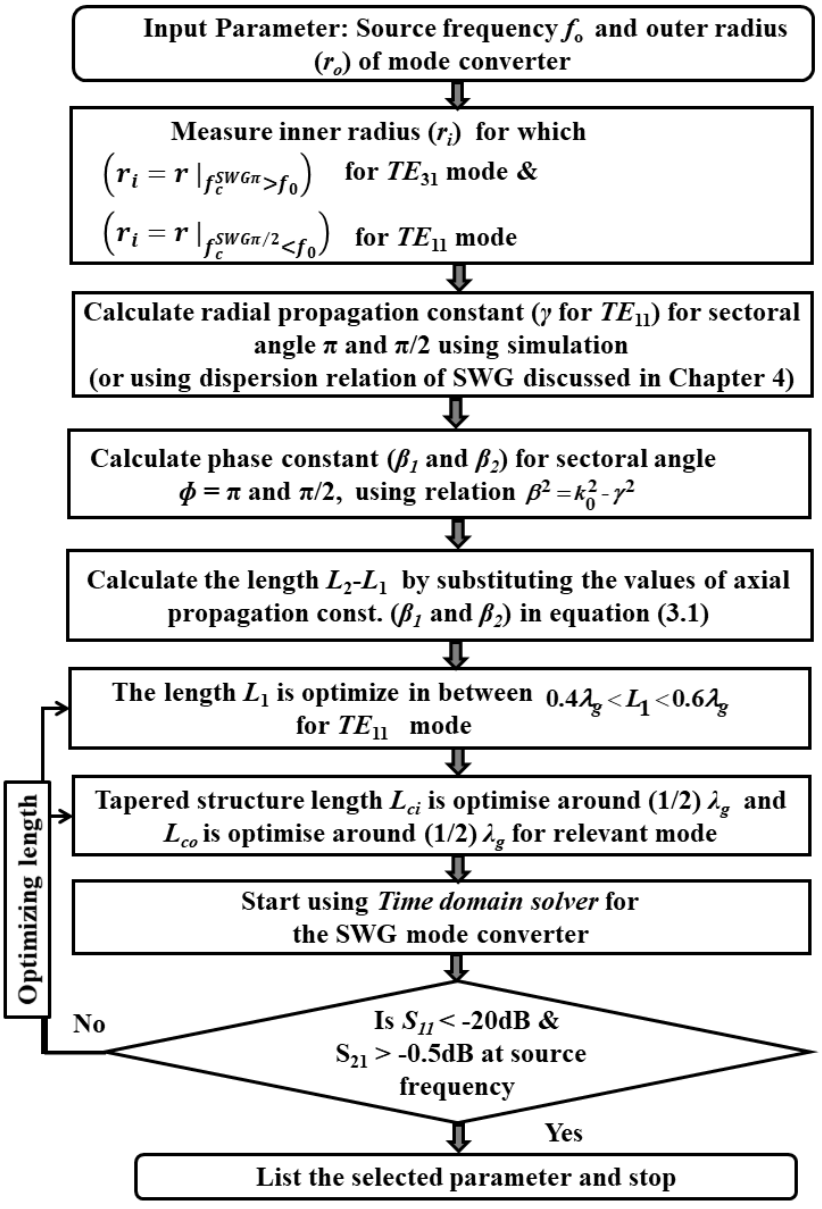

Figure 3.2. Design algorithm for the proposed TM_{01} to TE_{11} mode converter.

Table 3.2. SWG mode converter structure dimension.

Parameter	Values (mm)	Optimize Parameter	Values (mm)
L_2 - L_1	180.0	L_1	85.0
L_{mi}	26.0	L_{gi}	33.0
L_{mo}	26.0	L_{ci}	51.0
L_h	185.0	L_{co}	51.0
r_h	157.5		

3.2.Experimental Setup

Properly designed SWG mode converters can provide high mode conversion efficiency. Using the design approach described through the design algorithm, Figure 3.2, an S-band TM_{01} to TE_{11} SWG mode converter (input parameter listed in Table 3.1) is designed and optimized; designed parameters of the mode converter are listed in Table 3.2. The designed SWG mode converter fabricated using aluminium metal and fabricated mode converter is shown in Figure 3.3 (a,b). For the measurement of the microwave characteristics of the designed and fabricated SWG mode converter, a mode transducer is used to feed the RF-power in desired TM_{01} mode at its input port [Chittora *et al*. (2016)]. A conical horn antenna is used to radiate the RF power at the output port of mode converter.

For the conversion of the RF power output of the microwave signal generator, a mode transducer having monocone with a skirt in design has been fabricated as similar as reported in Chittora *et al*. (2016). This mode launcher converts the microwave signal generator output into TM_{01} mode over the circular waveguide at the desired frequency band of around 3 GHz. At the output side of the SWG mode converter, a conical horn antenna is connected to radiate the TE_{11} mode. The optimum performance on horn antenna has achieved by using it in coaxial form, where the tapered section of the inner

conductor near output port has been placed inside the conical horn antenna, as similarly reported in Yuan *et al*. (2006).

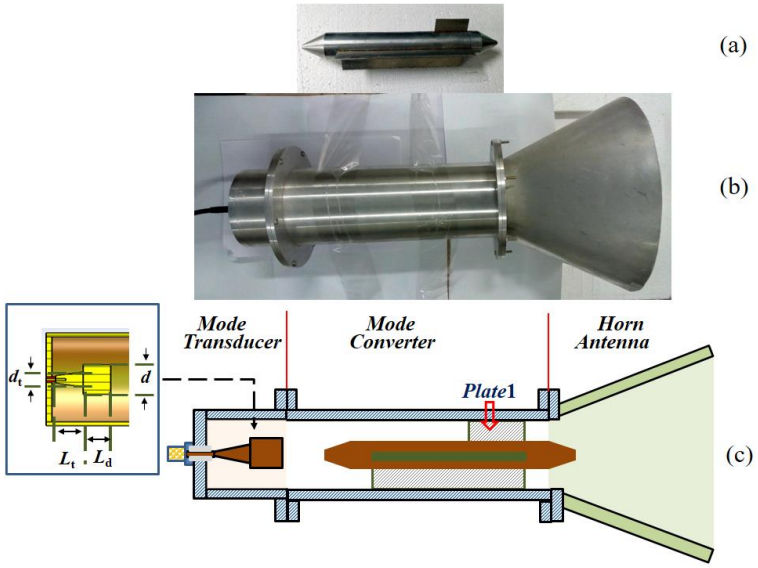

Figure 3.3. Typical model (a) Photograph of metallic plates fused with the inner conductor, (b) complete fabricated structure with a mode transducer and a conical horn antenna (c) simulated design of TM_{01} to TE_{11} SWG mode converter.

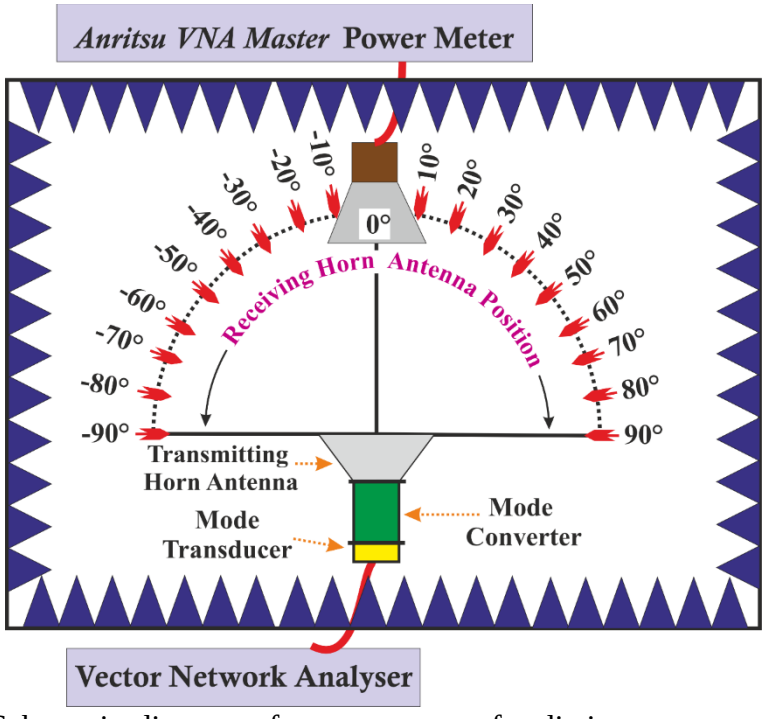

Figure 3.4. Schematic diagram of measurement of radiation pattern and identifying radiated mode by varying the azimuthal position of receiving antenna.

It is complicated to measure the modes experimentally and their energy proportion accurately for all possible modes at the output port. Also, there is no any

dedicated device present to sense the energy proportion accurately, the output modes of the mode converter are measured using far-field radiation measurement as similarly reported in Yuan *et al*. (2005, 2006). The complete schematic of the radiation pattern measurement setup is shown in Figure 3.4.

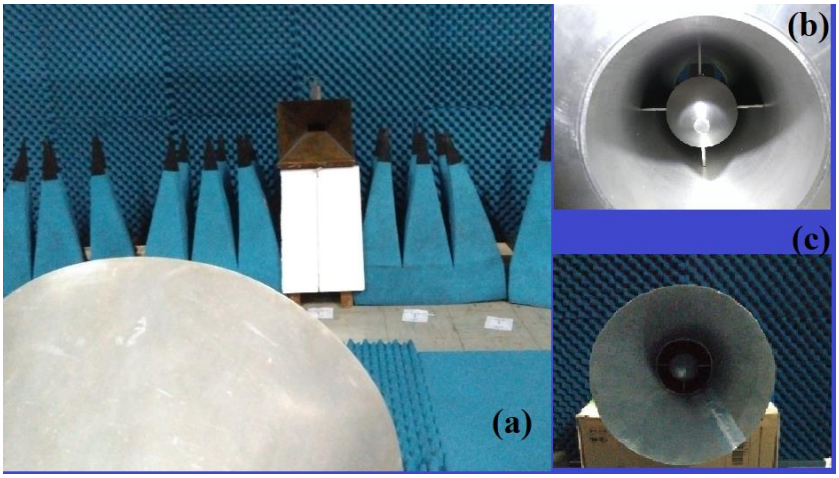

Figure 3.5. Snapshot of the experimental setup in a semi-anechoic chamber. (a) mode converter is at transmitting side, while an S-band standard horn antenna is at receiving side connected with a power meter, (b) tapered section and sectoral plates in SWG mode converter, (c) tapered section and conical horn antenna at transmitting side.

In the experiment, a Vector Network Analyser (VNA) is connected to a mode transducer and is supplying RF-power at frequency 3 GHz in TM_{01} mode. Calibration has been achieved using Anritsu TOSLNF50A-18 Calibration Kit, and by choosing calibration type *Full* S_{11} - *Port1* (S_{11}). A reflection coefficient (S_{11}) has been calculated using this VNA. Mode transducer is connected with SWG mode converter and followed by a conical horn antenna, where they are converting and radiating electromagnetic wave in TE_{11} mode. On the transmitting side, continuous wave signal of 13 dBm amplitude at 3 GHz is feed to mode launcher. Whereas on the receiving side standard S-band, a pyramidal horn antenna is connected with Anritsu VNA Master Power meter. The receiving antenna is of copper metal and has gain 15.9 dBi at frequency 3 GHz. The measurement is taken in the semi-anechoic chamber and is shown in Figure 3.5(a).

In the experiment, during the shifting of receiving antenna position, it is better to practice to switch the power supply for safety purpose and to avoid direct exposure to microwave radiation. Since the power meter cable is not very long, extra USB A-Male to A-Female extension cable is added, and to avoid any interference on cable joints, they are covered with microwave absorbing foam or sheet. Photograph of the fabricated tapered section and metallic plates is shown in Figure 3.5(b). Also, the tapered section and conical horn antenna at the outside of the SWG mode converter is shown in Figure 3.5(c). A SWG mode converter has designed, and its radiation pattern measurement is performed to validate the simulation results.

3.3. Results and Discussion

A modified all-metal SWG mode converter, for TM_{01} to TE_{11} mode conversion with high mode conversion efficiency, beam stability and suitable for the High Power microwave systems is proposed (Figure 3.1). As shown in Figure 3.1, the left side of the tapered section is providing the required mode conversion from TM_{01} to *TEM* mode along with the impedance matching whereas its right-side tapered section has used only for the impedance matching and to enhance to the directivity of the horn antenna. Inner conductor radius (r_i) and plate length $(L_2 - L_1)$, are the important parameter, where effective inner radius (r_i) ensures the propagation of TE_{11} mode in the SWGs and higher-order modes, e.g., TE_{21}, TE_{31} get attenuated. By substituting the values of axial propagation constant of two SWGs in equation (27), the plate length $(L_2 - L_1)$ is calculated. Following the design algorithm of SWG mode converter as shown in Figure 3.2, the designed mode converter got fabricated and is shown in Figure 3.5. The input parameters are given in Table 3.1 and the optimized structure dimensions are obtained using design algorithm tabulated in Table 3.2. The main difference between the

proposed design and the design reported by Yuan *et al*. (2005, 2006) are the removal of stubs and change in position of *Plate1* along with length optimization and is discussed later.

Simulation of the SWG mode converter along with a conical horn antenna has been performed using commercial software CST MICROWAVE STUDIO (CST MWS). Using Tables 3.1 and 3.2, the structure has been modelled and simulated, also the aluminium material is chosen for the metallic structure. The waveguide port has been applied at the input end of Region *I(a)* and the output end of Region *III(a)*. Using Time Domain Solver, the scattering parameters and radiation pattern have obtained for validation of experimental and analytical results.

Using electric field monitor at each junction, radial electric field vectors are observed, as shown in Figure 3.6. At the input end of Region *I(a)* and *I(c)*, electric field lines are in the same direction for a constant radius moving radially outward. It is visible from Figure 3.7, that the electric field lines at the input end of Region *II(a)* are moving radially outward but get separated between three SWGs. At input end of Region *II(b)*, these electric field lines of SWG_{π} are in the same direction as the previous, while for $SWG_{\pi/2}$ field lines have the opposite orientation. The electric field lines of SWG_{π} are also get separated in two $SWG_{\pi/2}$. Thus, field lines of four $SWG_{\pi/2}$ get combined at the output end of Region *II(b)* and constitute TE_{11} mode over the coaxial waveguide.

Bifurcation of SWG_{π} into $SWG_{\pi/2}$ has importance in mode converter design. TE_{11} mode propagating through SWG_{π} and $SWG_{\pi/2}$, after launching in the coaxial waveguide, excites the TE_{11} mode and TE_{21} mode. Whereas, two neighbouring $SWG_{\pi/2}$ having the same electric field orientation cancels the generation of TE_{21} mode in the coaxial waveguide and transfers its power in TE_{11} mode, as shown in Figure 3.7. As observed from Figure 3.7, the power from each $SWG_{\pi/2}$ (having only TE_{11} mode) is

converted to TE_{21} likeness mode over the coaxial waveguide. Due to the orthogonal orientation of TE_{21} likeness mode, they could not combine to excite TE_{21} mode over the Region *III*. So, after combining of field lines they excite only TE_{11} mode, as shown in Figure 3.7. Hence the position of *Plate1* plays a key role in avoiding the generation of the TE_{21} mode in Region *III*(a). Length of *Plate1* has been optimized near the length of half wavelength, to match the impedance. This reduces the design complexity by avoiding the stubs (used for impedance matching) in mode converter, as reported by Yuan *et al*. (2005, 2006). Also, Chittora *et al*. (2015) had decreased the dielectric size in the azimuthal direction, from semi-circular to arc, to stabilize the beam by equalizing the field content. Whereas in the proposed design, the position of *Plate1* provides beam stabilization as shown in Figure 3.8, where electric fields in the horn antenna are coming out with peak power stable along the axis of propagation. This ensures the operation of SWG mode converter to convert TM_{01} to TE_{11} mode. As a first test, working of SWG mode converter has been visualized, by examining the radiation pattern of the SWG mode converter with the cylindrical horn antenna.

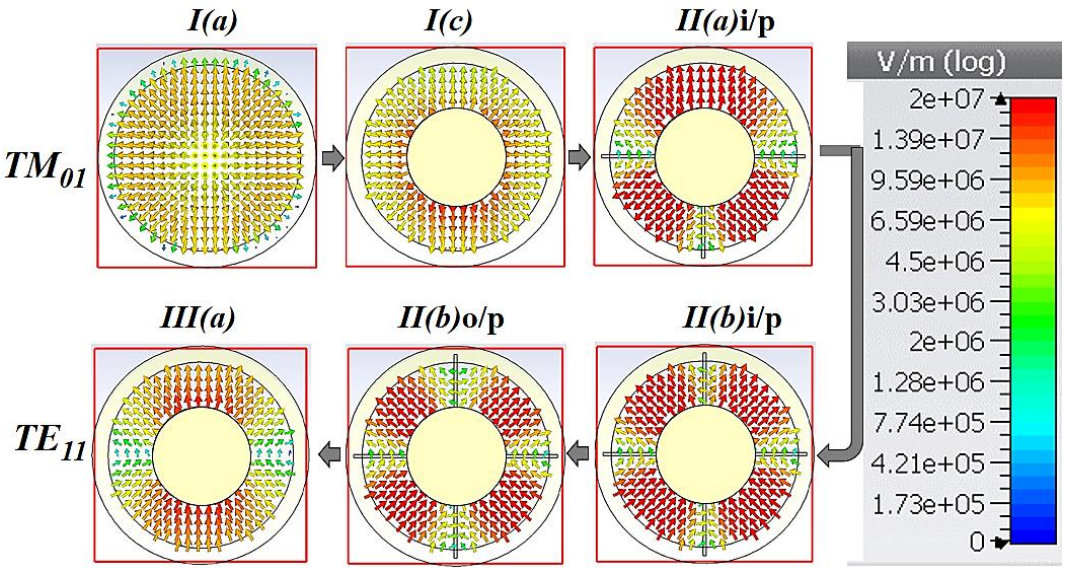

Figure 3.6. The procedure of mode conversion in SWG mode converter using *E* field monitors placed at different azimuthal positions in simulated design.

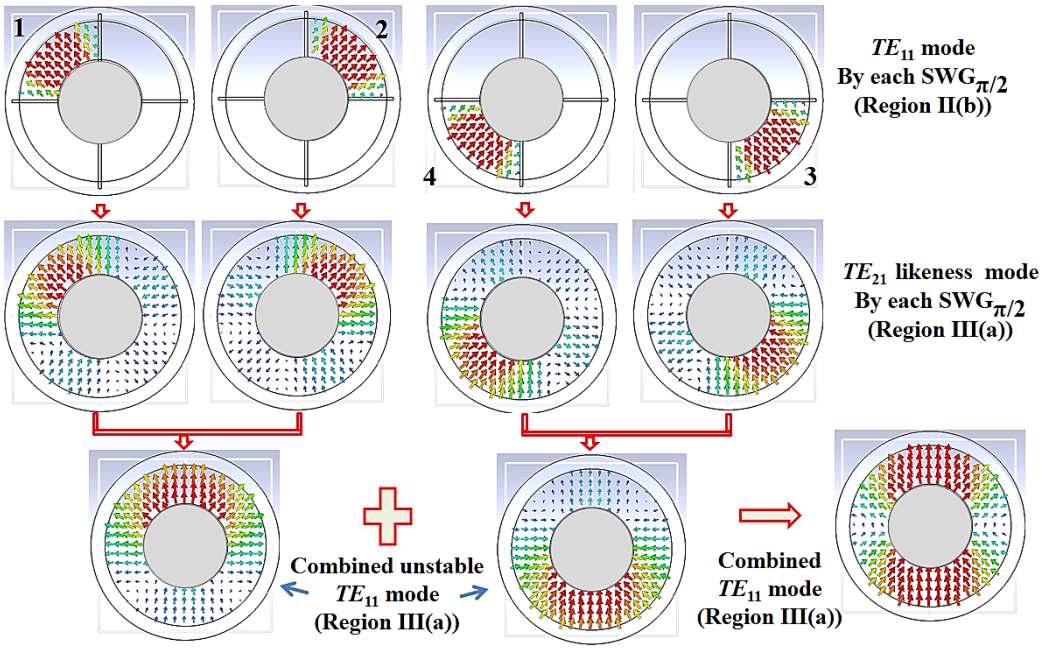

Figure 3.7. Combining electric fields through all $SWG_{\pi/2}$ (of Region *II(b)*) in the coaxial waveguide (of Region *III(a)*), and showing the advantage of using *Plate1* in the SWG mode converter.

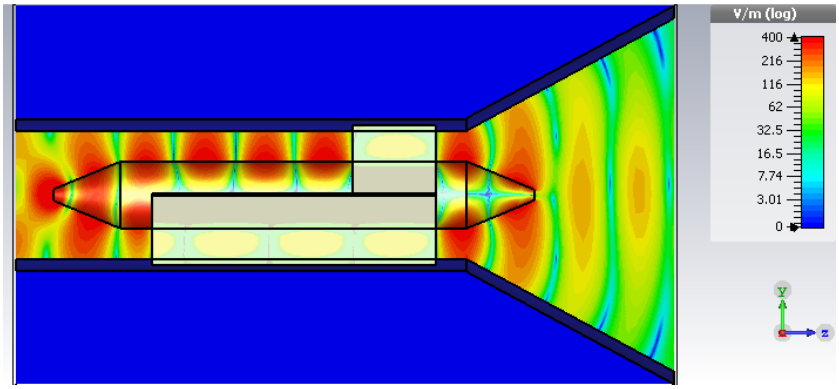

Figure 3.8. Simulated model of SWG mode converter with a contour plot of electric field distribution in x = 0 plane at frequency 3 GHz.

In Section 3.2, the experimental setup is explained, where using a pyramidal horn antenna is connected with a power meter, the radiation pattern of the SWG mode converter is obtained. The mode conversion is verified by experimental measurement of the far-field radiation pattern as similar experimental setup shown by Benford *et al.* (2007). Radiation pattern is plotted in H-plane, over the range of azimuthal angle -90° to 90°, as shown in Figures 3.9 and 3.10. The complete system with having mode

transducer, horn antenna and SWG mode converter are used in the experiment, as shown in Figure 3.3(c). During the experiment, microwave source is generating *TEM* mode and is converted to TM_{01} mode by using a mode transducer. This mode transducer is required as a feed for the SWG mode converter. This TM_{01} mode is converted to TE_{11} mode by using SWG mode converter and radiated with the help of horn antenna. The complete system measured without mode converter and with mode converter is shown in Figures 3.9 and 3.10, respectively. It is further observed from Figure 3.9, that the radiation intensity at 0° azimuthal angle, from the simulation, is -57.90 dBi and by the experiment is -15.51 dBi. Hence it proves that the launched mode by mode transducer as a feed of SWG mode converter is of TM_{01} mode because there is null at the azimuthal angle of 0°. Figure 3.10, exhibit the measured RF radiation pattern with the use of SWG mode converter and the radiation intensity at 0° azimuthal angle is 17.29 dBi from the simulation and is 20.57 dBi by the experiment. Chittora *et al*. (2015) has also reported a similar pattern to validate and compare the mode conversion. Also, Lee *et al*. (2004) and Yuan *et al*. (2005) had reported that the highest gain of TE_{11} mode at azimuthal angle 0°. The results shown as Figure 3.10, proves that the radiated mode with mode converter is of TE_{11} mode because the peak power is obtained from the azimuthal angle of 0°. Alignment of transmitting antenna and receiving antenna plays an important role in measuring directivity of fabricated heavyweight SWG mode converter. In the experiment, alignment is achieved with the help of thread and ruler. Comparing the results shows the evidence of mode conversion from TM_{01} mode to TE_{11} mode when mode converter is used. Due to scattering at the edge of the conical horn antenna, side lobes power do not occur significantly in the measured radiation pattern.

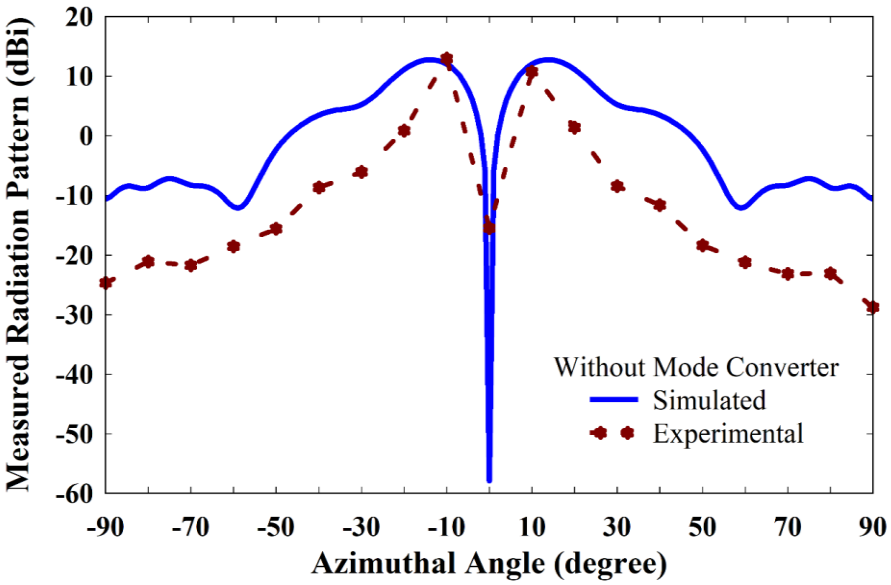

Figure 3.9. The radiation pattern obtained and measured for the system without using the SWG mode converter, and is showing the TM_{01} mode pattern from mode transducer.

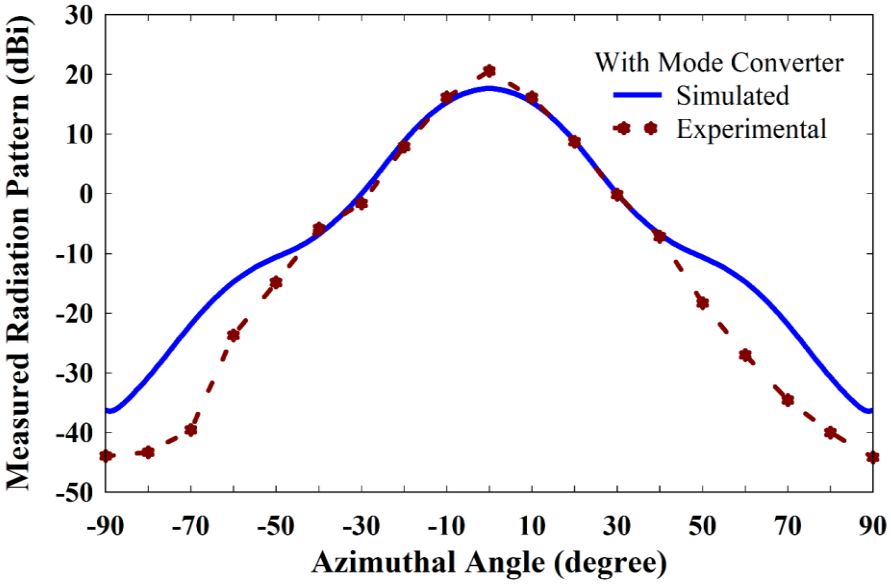

Figure 3.10. Comparison of radiation pattern measurement (in H-plane), using simulation and experiment form -90° to +90° azimuthal angle, keeping 0° as a boresight. The radiation pattern obtained and measured for the system with the SWG mode converter is showing the TE_{11} mode pattern.

The optimization achieves for the selection of the appropriate size of the inner conductor in the mode transducer. The optimized parameters of the inner conductor in the mode transducer are, $L_t = 25\,\text{mm}$, $d = 40\,\text{mm}$, $d_t = 24\,\text{mm}$. The mode transducer exhibit the return loss less than -20 dB for the frequency range 2.788 GHz to 3.098 GHz.

The mode transducer is also having very smooth mode launching capability with transmission loss -0.0281 dB at the required frequency (3 GHz) of SWG mode converter. In Figure 3.11, the performance of the mode transducer is visualizing and shows good performance of exciting the circular waveguide with a TM_{01} mode around frequency 3 GHz. The key idea behind the design of the mode transducer is to keep the azimuthal symmetry of *TEM* mode sustainable. Thus the deformed inner conductor is ended abruptly and used for matching the impedance between coaxial feed and circular waveguide. At the end of inner conductor coaxial waveguide *TEM* mode transformed to circular waveguide TM_{01} mode.

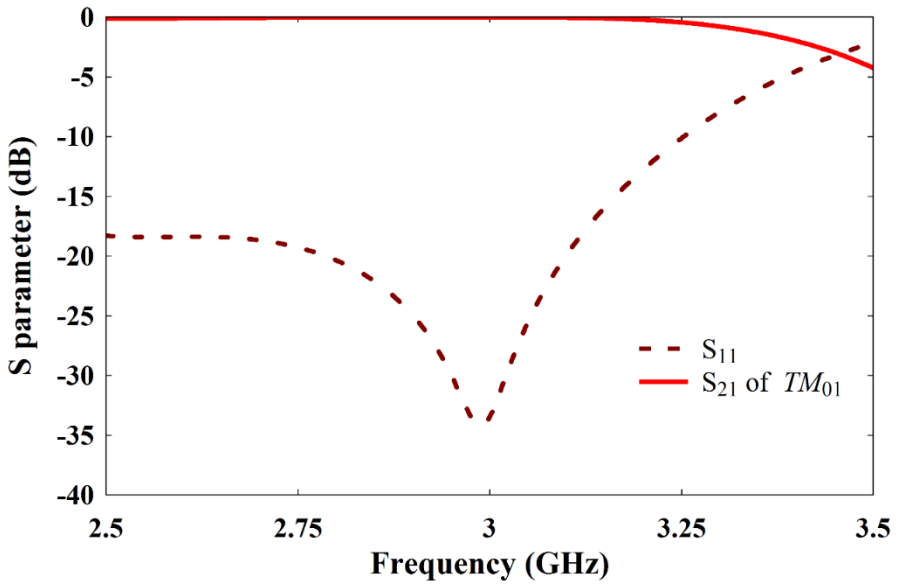

Figure 3.11. Performance evaluation of mode transducer using S-parameter.

In the simulated design 1.25 GW power of TM_{01} mode is feed at Port-1, and to verify the design scattering parameter is observed and compared with experimental results. This design is filled with vacuum and having a maximum electric field of 61.87 MV/m in z-plane. As shown in Figure 3.12, at the frequency 3 GHz, the return loss of the fabricated design is measured at the input port of mode launcher using Vector

Network Analyser, and the result is -22.57 dB and the simulation result is -22.38 dB. The comparison shows good agreement between experimental and simulation results, whereas the experimental result is obtained at the input port of mode launcher connected with the microwave source. This result shows, the proposed designing procedure of using optimize the length of *Plate1* is beneficial over the use of stub matching. Also, the interaction of stubs will create problems for the HPM sources which are not coaxial in the structure at the output end, e.g., RBWO, RKO and VIRCATOR, etc.

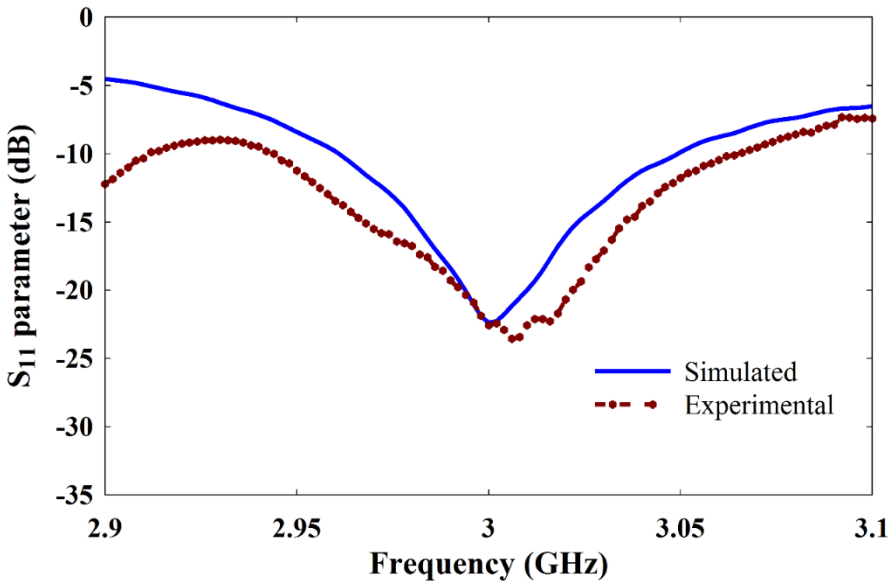

Figure 3.12. Comparison of reflection loss between simulated and measured at the input end of Region *I*(a) and the feed of mode transducer respectively.

The SWG mode converter performance is also analyzed in terms of its conversion efficiency, where it requires port at both ends. This is possible in simulated design with some changes (L_{co}= 38 mm, L_{mo}= 16.5 mm) in Region *III*. All the mode converter design conversion efficiency is calculated regarding the transmission scattering coefficient $|S_{21}|^2$, as shown in Figure 3.13, over the frequency range 2.9 GHz to 3.1 GHz. The conversion efficiency at frequency 3GHz, of the simulated design, is 98.42% for TM_{01} to TE_{11} mode, while the TM_{01} to *TEM* mode conversion efficiency is 0.14%. The results show higher mode conversion efficiency of the proposed mode

conversion at the operating frequency 3 GHz. The proposed design is examined here, and without any use of stubs the SWG mode converter is achieving significant mode conversion efficiency. Also, the use of *Plate1* ensures to get pure TE_{11} mode because it is creating four $SWG_{\pi/2}$ in that sectoral region, which further do not support the formation of TE_{21} mode. The SWG mode converter can be used in microwave heating too because it has the property to convert azimuthally symmetrical modes *TEM* or TM_{01} to the modes having maximum electric field strength at the axis of propagation (TE_{11} mode). Also, in space beam driven rocket proposed by Benford *et al*. (2007) does require confined and focused RF beam by HPM systems, in such areas of development an all-metal SWG mode converter is of vital use as well as importance.

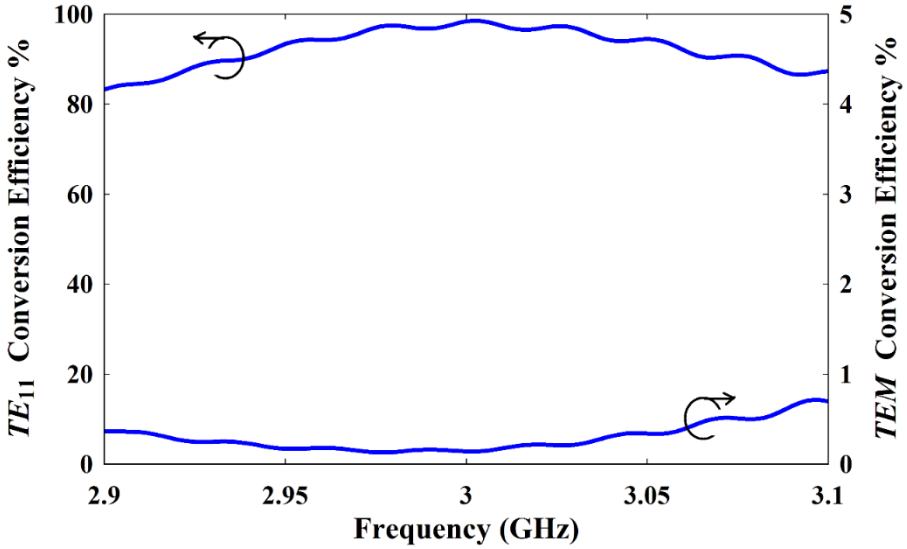

Figure 3.13. Mode conversion efficiency (in %) for desired TE_{11} mode and dominant mode *TEM* of the coaxial waveguide. The result is obtained in simulated design at the output end of Region *III*(a).

Tapering at both sides of TM_{01} to TE_{11} SWG mode converter, allows the mode converter design to be used with different HPM sources which generate TM_{01} mode. Also tapering of Region *I(b)* can be avoided using with HPM source MILO, which generates *TEM* mode, and similar reported by Yuan *et al*. (2005, 2006). An analytical study of the SWG mode converter is required for further investigation for its fast

designing and optimization. So, the investigation requires computational modelling with a different technique other than the technique used by commercial software CST Studio. The working behaviour of HPM sources in comparison to mode transducer should vary, so the performance of SWG mode converter with different HPM sources will be useful to examine for future research.

3.4.Conclusions

In order to overcome the high reflection and unstable radiating beam problems arises in the SWG mode converters; its *Plate1* length is optimized along with its positioning is also modified. For a favouring radiation pattern with and without SWG mode converter, the results obtained through CST simulation as well by the EM analysis and compared. It is established that the present design for TM_{01} to TE_{11} SWG mode converter eliminates stub matching requirement which further minimises the high variations in reflection losses. To validate our design methodology, the simulated results of reflection loss and radiation pattern are also compared with the experimental results and found in the agreement. The proposed all-metal SWG mode converter, its analysis, and design methodology would be useful for the HPM system developers. In the future, deep analytical study of SWG mode converter using computational modelling technique other than available commercial simulation software and its application-based study with different HPM sources will be useful for further research.

This work is extended further to develop a theory for characterization of mode converter. Mode matching techniques is used and the details are reported in next chapter, Chapter 4.